Coronal density diagnostics with Helium-like triplets: CHANDRA-LETGS observations of Algol, Capella, Procyon, epsilon Eri, alpha Cen A&B, UX Ari, AD Leo, YY Gem, and HR 1099

Ness, J.-U.; Schmitt, J.H.M.M.; Burwitz, V.; Mewe, R.; Raassen, A.J.J.; van der Meer, R.L.J.; Predehl, P.; Brinkman, A.C.

Published in:
Astronomy & Astrophysics

DOI:
10.1051/0004-6361:20021146

A&A 394, 911–926 (2002)
DOI: 10.1051/0004-6361:20021146

Astronomy & Astrophysics

Coronal density diagnostics with Helium-like triplets: CHANDRA–LETGS observations of Algol, Capella, Procyon, ϵ Eri, α Cen A&B, UX Ari, AD Leo, YY Gem, and HR 1099

J.-U. Ness[1], J. H. M. M. Schmitt[1], V. Burwitz[2], R. Mewe[3], A. J. J. Raassen[3,4], R. L. J. van der Meer[3], P. Predehl[2], and A. C. Brinkman[3]

[1] Universität Hamburg, Gojenbergsweg 112, 21029 Hamburg, Germany
[2] Max-Planck-Institut für Extraterrestrische Physik (MPE), Postfach 1603, 85740 Garching, Germany
[3] Space Research Organization Netherlands (SRON), Sorbonnelaan 2, 3584 CA Utrecht, The Netherlands
[4] Astronomical Institute "Anton Pannekoek", Kruislaan 403, 1098 SJ Amsterdam, The Netherlands

Received 24 April 2002 / Accepted 1 August 2002

Abstract. We present an analysis of ten cool stars (Algol, Capella, Procyon, ϵ Eri, α Cen A&B, UX Ari, AD Leo, YY Gem, and HR 1099) observed with the Low Energy Transmission Grating Spectrometer (LETGS) on board the *Chandra* X-ray Observatory. This sample contains all cools stars observed with the LETGS presently available to us with integration times sufficiently long to warrant a meaningful spectral analysis. Our sample comprises inactive, moderately active, and hyperactive stars and samples the bulk part of activity levels encountered in coronal X-ray sources. We use the LETGS spectra to carry out density and temperature diagnostics with an emphasis on the H-like and the He-like ions. We find a correlation between line flux ratios of the Ly$_\alpha$ and He-like resonance lines with the mean X-ray surface flux. We determine densities using the He-like triplets. For all stars we find no significant deviations from the low-density limit for the ions of Ne, Mg, and Si, while the measured line ratios for the ions of C, N, and O do show evidence for departures from the low-density limit in the active stars, but not in the inactive stars. Best measurements can be made for the O VII triplet where we find significant deviations from the low-density limit for the stars Algol, Procyon, YY Gem, ϵ Eri, and HR 1099. We discuss the influence of radiation fields on the interpretation of the He-like triplet line ratios in the low-Z ions, which is relevant for Algol, and the influence of dielectronic satellite lines, which is relevant for Procyon. For the active stars YY Gem, ϵ Eri, and HR 1099 the low f/i ratios can unambiguously be attributed to high densties in the range $1–3\times10^{10}$ cm^{-3} at O VII temperatures. We find our LETGS spectra to be an extremely useful tool for plasma diagnostics of stellar coronae.

Key words. atomic data – techniques: spectroscopic – stars: coronae – stars: late-type – stars: activity – X-rays: stars

1. Introduction

The coronal X-ray emission from the Sun is spatially correlated with photospheric regions exhibiting magnetic field concentrations. Therefore spatially unresolved X-ray emission from other solar-like stars is commonly used as a tracer for stellar magnetic activity. The specific advantage of X-ray measurements is that any stellar X-ray emission exclusively comes from the corona, and unlike other activity tracers, is not affected by photospheric emissions, rapid rotation, turbulent broadening etc. X-ray observations of stars carried out with the *Einstein Observatory* (cf. Vaiana et al. 1981) and with ROSAT (Schmitt 1997) revealed the ubiquity of stellar X-ray emission among stars placed in the Hertzsprung-Russell diagram. The extensive ROSAT surveys showed that essentially all late-type solar-like stars with outer convection are surrounded by hot ($T \geq 1$ MK) coronae (Schmitt 1997). The X-ray luminosity of a given type of star can vary over four orders of magnitude over our sample, and rotation appears to be the most important parameter characterizing the level of X-ray emission of cool stars (cf. Pallavicini et al. 1981). The solar corona as observed with modern X-ray and XUV telescopes on board YOHKOH, SOHO, or TRACE is found to be extremely structured, and even in the high angular resolution TRACE images there appears to be spatially unresolved fine structure. Yet spatially resolved X-ray observations of stellar coronae are currently not feasible. Information on the spatial structure of stellar coronae can in principle be derived from X-ray light curves of suitably chosen stars such as eclipsing binaries, yet the actual information derivable from such data is rather limited; a discussion of the pre-XMM and pre-*Chandra* results together with the difficulties and limitations of light curve inversions is given by Schmitt (1998).

How do stars manage to produce far more X-ray output than the Sun? One of the basic assumptions used in the interpretation of stellar X-ray emission is that the building blocks, the solar corona is composed of, are also those that make up the

Send offprint requests to: J.-U. Ness,
e-mail: jness@hs.uni-hamburg.de

X-ray emission of stars. This assumption can only be tested by spectroscopic investigations. The *Einstein Observatory* and ROSAT provided data with rather modest spectral resolution. A few measurements of selected stars were carried out with the transmission gratings available on board of the *Einstein* and EXOSAT satellites. Higher spectral resolution information, albeit only at wavelengths longward of 90 Å, but not in the X-ray range, was provided by the EUVE spectrometers. The low resolution proportional counter spectra obtained with the *Einstein* and ROSAT satellites were fitted with plasma emission models in order to derive plasma temperatures and emission measures (see, for example, Schmitt et al. 1990); later also elemental abundances were included as fit parameters (see, for example, Antunes et al. 1994). However, the previous measurements did not allow measuring densities n_e and emission measures EM independently, such that no emitting volumes V could be estimed from $EM = n_e^2 V$. Therefore no information about loop sizes was accessible. With the new high resolution spectra obtained with the *Chandra* and XMM-Newton grating spectrometers it is possible for the first time to measure individual lines in the X-ray range with reasonable effective areas over a wide bandpass for a larger sample of stars in the same fashion as X-ray emission lines from the solar corona have been obtained and analyzed for many years (e.g., Doyle 1980; McKenzie & Landecker 1982; Gabriel et al. 1988). Specifically, He-like triplets can be observed for a variety of elements (carbon, nitrogen, oxygen, neon, magnesium, and silicon) and stars. The theory of He-like triplets can be tested in active and inactive stars and density information can be derived; this information can be supplemented by other line ratios, e.g., Fe XXI lines (measured with the LETGS), which also yield density constraints. The density-sensitive line ratios are the missing link relating emission measure and volumes. Further, emission measure weighted "effective" temperatures can be derived from suitable line ratios, in particular the ratios between the Ly$_\alpha$ and He-like resonance lines.

First results from XMM-RGS measurements were presented by, e.g., Audard et al. (2001a, 2001b) and Güdel et al. (2001a, 2001b) with special focus on global modeling techniques to derive temperature distributions and abundances for the Castor system, Capella, AB Dor, and HR 1099. Measurements with the MEG on board *Chandra* were presented by, e.g., Canizares et al. (2000), Ayres et al. (2001), and Phillips et al. (2001). The MEG and HEG provide the highest resolution at energies >1 keV and Brickhouse et al. (2001) report the measurements of orbit related line shifts in 44 Boo, thus eventually opening up the road to X-Ray Doppler imaging of stellar coronae. Plasma diagnostics carried out with LETGS spectra were presented by, e.g., Mewe et al. (2001) on Capella, Ness et al. (2001a) on Capella and Procyon, and Ness et al. (2002a) on Algol; these authors use line ratios in order to derive plasma densities and temperatures.

The purpose of this paper is to summarize results from recent LETGS measurements of a set of ten cool stars with a special focus on the density diagnostics with He-like triplets. Albeit some results on He-like triplets were published earlier (e.g., Ness et al. 2001a; Mewe et al. 2001; Ness et al. 2002a; Stelzer et al. 2002; Raassen et al. 2002a; Audard et al. 2001c), we will use these already published results for comparison with our new results on UX Ari, ϵ Eri, α Cen A and B, and AD Leo, which are presented here for the first time.

The specific information that can be derived from He-like line ratios is the plasma density. The theory of such triplets is described extensively in the literature; we refer to Gabriel & Jordan (1969), who developed the theory, and to Blumenthal et al. (1972), Mewe & Schrijver (1978), Pradhan et al. (1981), Pradhan & Shull (1981), and recently Porquet et al. (2001), who refined and revised the theory. In this paper we use the relation

$$\frac{f}{i} = \frac{R_0}{1 + \phi/\phi_c + n_e/N_c}, \quad (1)$$

denoting the forbidden line with f and the intercombination line with i with the low density limit R_0, the radiation term ϕ/ϕ_c (the values derived in Sect. 5.1 are listed in Tables 5 to 7), and the electron density n_e; N_c is the so-called critical density, which leads to an f/i-ratio just in between the high- and low-density limits. Thus, given an X-ray measurement of the f/i-ratio and knowledge of R_0, N_c, and ϕ/ϕ_c from other sources, the plasma electron density n_e can be inferred.

Our paper will be structured as follows: we first give a short description of the instrument with its capabilities and provide an overview of our sample of stars. We then introduce the new spectra and give a detailed description of the analysis presenting the measured line counts and describing the methods applied to analyze the obtained results. Our results of total X-ray luminosities, temperatures, and He-like densities for the ions Si XIII, Mg XI, Ne IX, O VII, N VI, and C V will be presented in Sect. 5. Our conclusions are given in Sect. 6.

2. The instrument

The new generation of X-ray telescopes and X-ray spectrometers on board *Chandra* and XMM-Newton has opened the world of spectroscopy to X-ray astronomy with specific emphasis on sensitivity (XMM-RGS) and spectral resolution (*Chandra* LETGS and HETGS). Spectroscopic measurements can be performed with both instruments using the Reflection Grating Spectrometer (RGS) on board XMM and the High Energy Grating (HEG), Medium Energy Grating (MEG), and the Low Energy Transmission Grating (LETGS) on board *Chandra*. While RGS, HEG, and MEG provide large effective area for high energies in the range 5 to 40 Å with high resolution, the LETGS covers a much larger wavelength range from 5–175 Å with high spectral resolution encompassing both the ROSAT bandpass (5–124 Å) and the *Einstein* bandpass (3–84 Å). As a result of this large band pass X-ray fluxes and X-ray luminosities corresponding to ROSAT or *Einstein* band passes can be measured from the LETGS data without the use of any plasma emission model by simply integrating the photon energies over all wavelength bins covering the corresponding wavelength ranges (cf. Sect. 4.2); the only corrections to be applied are those from interstellar absorption which are rather small for nearby stars. We further note that in the long wavelength region the spectral resolution of the LETGS even exceeds the spectral resolutions of the other

Table 1. Summary of stellar properties and measurement of X-ray luminosities for the stars. Effective areas are taken from Pease et al. (2000). ROSAT measurements are taken from, e.g., Hünsch et al. (1999, 1998). References for stellar radii and distances are given with superscripts.

	Algol	Capella	Procyon	ϵ Eri	α Cen		UX Ari	AD Leo	YY Gem	HR 1099
					A	B				
HD	19356	34029	61421	22049	128620	128621	21242	Gl388	60179C	22468
Spectr. Type	K2IV	G1III+G8 /K0III	F5 IV-V	K2V	G2V	K0V	G5V/K0IV	dM4.5Ve	dMIe/dMIe	K1IV/G5IV
d/pc	28[4]	13[7]	3.5	3.22	1.34		50[7]	4.9	14.7	28.97
$R_\star/R_\odot$	3.5[5]	9.2[1]	2.06[2]	0.81[3]	1.23[6]	0.80[6]	0.93/>4.7[7]	0.5	0.66/0.58	3.9/1.3
$t_{\rm exp}$/ksec	81.4	218.5	140.7	108.0	81.5		112.76	48.5	59	97.5
[a]$L_{\rm X}$ [10^{28} erg/s]	1444	255	2.43	20.9	0.65	0.52	2302	6.7	54.4	1585.6
[a]$F_{\rm X}$ [10^5 erg/cm^2/s]	191.4	4.89	0.93	51.73	0.70	1.32	169.24	43.52	245.4	169.3
[b]$L_{\rm X}$[10^{28} erg/s]	1101	239	1.64	2.22	0.30	0.26	1539	5.7	46.8	1156.2
ROSAT [10^{28} erg/s]	661	419.16	1.9	2.1	0.13[d]	0.20[d]	1205	7.22	82.37	1512.1
[c]$L_{\rm X}$[10^{28} erg/s]	1262	219	0.86	1.85	0.17	0.14	1716	5.0	45.7	1273.8
Einstein [10^{28} erg/s]	371	281	1.21	1.47	0.12[e]	0.28[e]	2900	8.32	21.5	700

[a]Range 0.07–2.5 keV (LETGS range: 5–175 Å).
[b]Range 0.1–2.4 keV (ROSAT range: 5.2–124 Å).
[c]Range 0.15–4 keV (*Einstein* range: 3–83 Å).
[d]Schmitt et al. (1998), ASP Conf., 154, 463.
[e]Golub et al. (1982), ApJ, 253, 242.

[1]Hummel, C. A., Armstrong, J. T., Quirrenbach, A., et al. 1994, ApJ, 107(5), 1859.
[2]Irwin, A. W., Fletcher, J. M., Yang, S. L. S., et al. 1992, PASP, 104, 489.
[3]Noyes, R. W., Baliunas, S. L., Belserene, E., et al. 1984, ApJ, 285, L23.
[4]Perryman, M. A. C., Lindegren, L., Kovalevsky, J., et al. 1997, A&A, 323, L49.
[5]Richards, M. T. 1993, ApJ, 86, 255.
[6]Soderblom 1986, A&A, 158, 273.
[7]Strassmeier, K. G., Hall, D. S., Fekel, F. C., et al. 1993, A&A, 100, 173.

instruments. One specific advantage of the LETGS resulting from its large wavelength range covered is the fact that the O VII triplet at around 22 Å, the N VI triplet at around 29 Å, and the C V triplet at around 41 Å can all be measured in one spectrum. The O VII triplet is covered by all instruments, but the MEG effective area is already small and steeply falling over the O VII triplet region. The N VI triplet is covered by the XMM-RGS and the LETGS, the C V triplet is only covered by the LETGS as well as the long wavelengths >100 Å which contain a number of lines from highly ionized Fe ions. This range was used by, e.g., Mewe et al. (2001) and Ness et al. (2002a) for an independent density analysis with Fe XXI line ratios (cf. Mason et al. 1984).

3. The sample of stars

The properties of our sample stars are summarized in Table 1; we also provide previously measured X-ray luminosities as well as the X-ray luminosities derived from our LETGS observations. As is clear from Table 1, our sample of stars comprises a wide range of X-ray luminosities $L_{\rm X}$ from few 10^{27} up to 10^{32} erg/s, which in fact covers almost the whole range of X-ray luminosities encountered for cool stars. The sample consists of three rather inactive dwarf stars in the immediate solar neighborhood, i.e., α Cen A and B and Procyon, of the active late-type dwarf stars AD Leo, YY Gem, and ϵ Eri, and of the active binary systems Algol, Capella, HR 1099, and UX Ari, where rapidly rotating evolved stars are responsible for the observed activity. We note in passing that the LETGS spectrally resolved α Cen A and B for the first time. A detailed analysis of this spectrum will be presented by Raassen et al. (2002b).

4. Observations and data analysis

4.1. Data extraction and reference to previous work

All the LETGS datasets were processed using the standard pipeline processing. The extraction of the spectra from the microchannel plate and the determination of the instrumental background are preformed in the same fashion as described by Ness et al. (2001a). The right and left dispersed spectra were co-added in order to increase the signal-to-noise ratio; this procedure is justified by Ness et al. (2001a) using Gaussian profiles. The number of counts in the individual lines is obtained with the CORA program (Ness & Wichmann 2002) developed and described by Ness et al. (2001a). The effective areas used for converting counts into fluxes were provided by Deron Pease (Oct. 2000) and all fluxes derived in this paper are based on this calibration.

In this paper we use the results obtained for Procyon and Capella by Ness et al. (2001a) for oxygen, nitrogen, and carbon, but corrected for new effective areas. The higher ionization stages for Capella have been analyzed by Mewe et al. (2001), but we re-analyze these ions using the larger set of available observations as listed in Ness et al. (2001a) and revising the results with the more recent effective areas; this reanalysis also ensures the maximally possible uniformity in data reduction. The results for Algol are taken from Ness et al. (2002a) without any further correction except for Ne IX. The analysis of the Ne IX triplet is new for all the stars except for Algol. In this

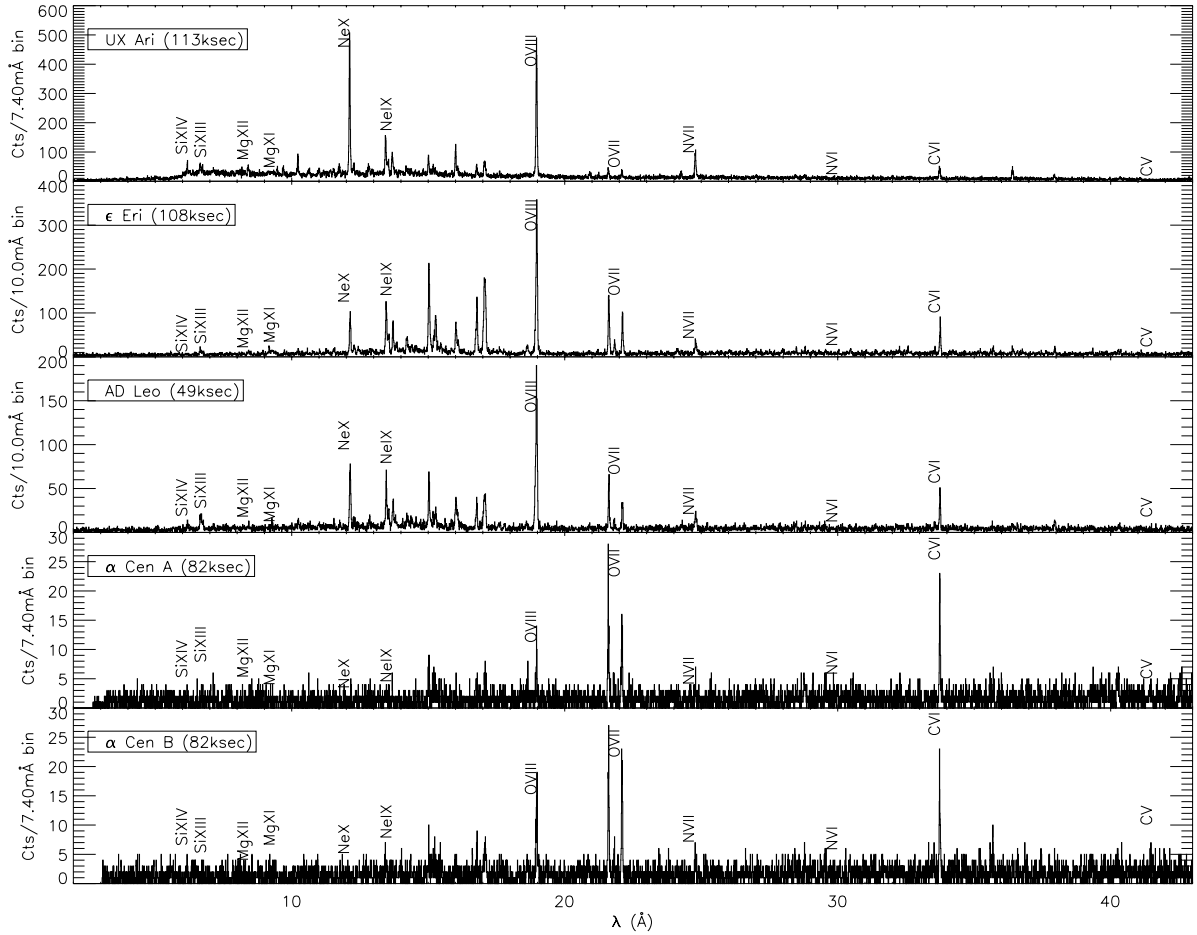

Fig. 1. The LETGS spectra of UX Ari, ϵ Eri, AD Leo, and α Cen A and B in the range 1–40 Å with all lines used in this paper marked. The instrumental background is subtracted.

paper we use a different approach and apply this procedure to Algol as well. We list all H-like and He-like results for the purpose of comparison in Tables 2 and 3.

4.2. The spectra

The new spectra obtained with the LETGS are shown in Fig. 1 for the stars UX Ari, ϵ Eri, AD Leo, and α Cen A and B in the wavelength range 1–40 Å. The instrumental background has been subtracted, i.e., the pure continuum plus line emission is shown in units of counts per bin; no corrections for the effective areas of the LETGS have been applied. As can be seen from an inspection of Fig. 1, the LETGS spectra of our sample stars differ considerably. Considerable continuum emission is detected for the active stars UX Ari, ϵ Eri, and AD Leo in the wavelength range 10 Å–20 Å, where the effective LETGS area is largest, while for α Cen A and B most of the emission is found in spectral lines. Strong emission lines from O, Fe, Si, Ne, and Mg are seen for UX Ari, AD Leo, and ϵ Eri in the wavelength range 10 Å–20 Å, while for α Cen A and B the O VII line at 21.6 Å is stronger than the O VIII line at 18.97 Å. In the long wavelength region, the prominent Fe IX at 171 Å is found to be the strongest line in α Cen A and B, while it is not detected in the spectra of ϵ Eri, AD Leo, and UX Ari. Instead we find highly ionized Fe ions from Fe XVIII (94 Å) up to Fe XXIII (e.g., 132 Å) in the UX Ari spectrum but not for ϵ Eri and AD Leo.

From Fig. 1 it is clear that isolated lines can be measured and line ratios can be calculated. In addition, broad band X-ray luminosities can be computed in the following way: the number of photons in a wavelength bin is converted to an energy flux by multiplying with $hc/\lambda A_{\rm eff}$ with h the Planck constant, c the speed of light, $A_{\rm eff}(\lambda)$ the wavelength-dependent effective area. Total X-ray luminosities in a given band pass are obtained by summing all energy fluxes calculated within the corresponding bins and dividing by $4\pi d^2$ (d is distance). Surface fluxes $F_{\rm X}$ are calculated from $F_{\rm X} = L_{\rm X}/4\pi R_\star^2$ with $R_\star$ denoting the stellar radius. The X-ray luminosities and surface fluxes obtained in this fashion are listed in Table 1 for all sample stars.

4.3. Measurement of line fluxes

The counts measured in emission lines are obtained using the CORA line fitting tool, which has been developed and applied by Ness et al. (2001a); a detailed description with examples is given by Ness & Wichmann (2002). The raw counts obtained with CORA represent the fitted number of expected counts for a given background. Measurement errors are given as $1\,\sigma$ errors and include statistical errors and correlated

Table 2. Measured line counts for the low temperature H-like and He-like ions O, N, and C (cf. Sect. 4.3).

	O		N		C	
	VIII	VII	VII	VI	VI	V
λ/Å	18.97	21.6/21.8/22.1	24.74	28.8/29.1/29.5	33.74	40.3/40.7/41.5
$A_{\rm eff}$/cm^2	24.31	15.6/15.34/15.32	15.26	13.9/13.6/13.9	11.59	4.9/3.36/3.24
Algol (r)	2882.96 ± 57.81	262.49 ± 22.6	1119.05 ± 38.38	141.33 ± 21.10	<50	–
(i)		128.77 ± 18.70		188.23 ± 25.53		–
(f)		120.90 ± 18.00		37.50 ± 14.31		–
Capella (r)	14676.8 ± 124.3	3071.2 ± 56.0	2280.3 ± 53.6	491.2 ± 31.49	2151.1 ± 51.3	440.7 ± 26.9
(i)		544.8 ± 31.4		228.2 ± 26.5		101.3 ± 18.24
(f)		2135.2 ± 51.1		384.5 ± 29.4		160.2 ± 22.37
Procyon (r)	673 ± 27.6	731.6 ± 28.7	206.9 ± 16.95	200.2 ± 16.8	697.5 ± 28.1	203.8 ± 17.0
(i)		203.0 ± 16.8		77.4 ± 12.3		123.1 ± 14.2
(f)		652.4 ± 27.3		97.1 ± 13.2		63.4 ± 13.5
ϵ Eri (r)	2025.8 ± 46.10	697.02 ± 27.70	178.85 ± 15.85	49.97 ± 9.52	289.88 ± 18.66	51.83 ± 9.63
(i)		153.61 ± 14.85		22.86 ± 7.95		16.42 ± 7.17
(f)		453.99 ± 22.78		24.41 ± 7.93		<12
α Cen A (r)	60.23 ± 8.63	115.93 ± 11.46	17.67 ± 4.96	38.40 ± 7.53	117.65 ± 11.44	39.38 ± 8.41
(i)		23.57 ± 6.01		16.79 ± 5.40		6.4 ± 5.3
(f)		89.68 ± 10.24		34.63 ± 7.48		12.98 ± 11.44
α Cen B (r)	124.18 ± 11.98	141.27 ± 12.55	32.07 ± 6.89	23.43 ± 6.06	102.86 ± 11.26	26.71 ± 7.40
(i)		24.42 ± 5.88		10.39 ± 6.47		6.47 ± 5.19
(f)		137.66 ± 12.34		20.12 ± 6.10		20.69 ± 7.51
UX Ari (r)	3207.85 ± 59.61	233.27 ± 21.11	602.85 ± 27.97	96.88 ± 15.62	309.36 ± 20.95	–
(i)		<30		27.17 ± 12.94		–
(f)		156.50 ± 18.41		36.13 ± 13.16		–
AD Leo (r)	1238.35 ± 36.40	263.97 ± 17.47	146.37 14.41	28.25 ± 7.89	203.41 ± 15.54	31.72 ± 8.44
(i)		53.01 ± 9.21		19.85 ± 8.28		–
(f)		170.31 ± 14.52		19.91 ± 7.89		–
YY Gem (r)	971.47 ± 32.27	193.31 ± 15.47	115.51 ± 13.20	–	149.44 ± 14.01	–
(i)		50.64 ± 9.63		–		–
(f)		115.75 ± 12.44		–		–
HR 1099 (r)	5584.06 ± 78.60	470.36 ± 27.81	502.08 ± 29.3	–	627.76 ± 29.63	–
(i)		114.74 ± 18.72		–		–
(f)		254.09 ± 22.44		–		–

errors in cases of line blends, but do not include systematic background errors. The raw counts obtained in this fashion are listed in Table 2 for the Ly$_\alpha$ lines and He-like triplets of oxygen, nitrogen, and carbon, and in Table 3 for the Ly$_\alpha$ lines and He-like triplets of neon, magnesium, and silicon. An inspection of Table 2 shows that the O VIII Ly$_\alpha$ line as well as the resonance line in the O VII triplet has been detected in all sample stars. Nitrogen is detected in all stars, but N VI has not been detected in YY Gem and HR 1099. In Algol no carbon lines have been detected (cf. Schmitt & Ness 2002), while the carbon Ly$_\alpha$ line at 33.74 Å has been detected in all other stars. The interpretation of data on the C V triplet is complicated; the effective area of the LETGS is rather small in this region and further, for the active stars, third order blending occurs with the neon triplet and Fe XVII/XIX lines; still we find emission from the C V resonance line at 40.3 Å in all cases but Algol, HR 1099, and YY Gem. In Table 3 we summarize our results for H-like and He-like lines of neon, magnesium, and silicon. Note that in the (under-exposed) spectra of α Cen A and B none of these lines has been detected, while in the much better exposed spectrum of Procyon the Ne IX triplet is clearly seen, but Ne X is very weak. In all other stars we find emission from both the H-like and He-like ions from neon and silicon, however, magnesium is very weak in most of the stars.

Table 3. Measured line counts for the highly ionized H-like and He-like ions Si, Mg, and Ne (cf. Sect. 4.3).

	Si		Mg		Ne	
	XIV	XIII	XII	XI	X	IX
λ/Å	6.18	6.65/6.69/6.74	8.42	9.17/9.23/9.31	12.14	13.45/13.55/13.7
$A_{\rm eff}$/cm^2	35.93	37.54/37.4/37.17	32.3	27.7/27.45/27.25	24.96	26.15/26.23/26.29
Algol (r)	658.32 ± 35.06	480.7 ± 35.95	578.04 ± 33.13	224.12 ± 26.15	2481.48 ± 56.31	631.23 ± 36.62
(i)		86.40 ± 33.10		84.85 ± 23.29		80.52 ± 30.74
(f)		314.10 ± 30.60		76.09 ± 22.80		347.91 ± 31.94
Capella (r)	679.72 ± 31.83	2487.72 ± 66.56	1682.28 ± 47.12	2654.49 ± 60.12	6479.41 ± 88.70	3960.85 ± 79.78
(i)		307.16 ± 62.44		481.71 ± 38.70		1109.18 ± 64.76
(f)		1346.19 ± 48.71		1452.03 ± 47.24		2312.77 ± 66.94
Procyon (r)	–	–	–	–	10.67 ± 4.87	66.93 ± 10.46
(i)		–		–		13.55 ± 6.63
(f)		–		–		35.03 ± 8.47
ϵ Eri (r)	<19	62.81 ± 11.75	45.05 ± 9.96	68.83 ± 11	480.78 ± 24.0	564.02 ± 27.20
(i)		13.47 ± 10.6		27.93 ± 9.1		116.91 ± 17.64
(f)		37.55 ± 9.82		44.09 ± 9.8		347.98 ± 22.35
UX Ari (r)	315.75 ± 26.17	321.13 ± 36.61	165.18 ± 20.70	47.54 ± 17.63	3038.04 ± 58.74	873.08 ± 35.98
(i)		48.81 ± 39.98		<25		187.82 ± 25.50
(f)		146.42 ± 27.54		29.62 ± 16.78		465.67 ± 29.87
AD Leo (r)	52.06 ± 9.38	81.35 ± 12.93	17.18 ± 5.6	–	407.87 ± 21.82	276.32 ± 19.20
(i)		34.66 ± 12.31		–		73.3 ± 13.69
(f)		45.55 ± 10.02		–		165.42 ± 16.04
YY Gem (r)	72.49 ± 11.06	82.50 ± 12.93	44.58 ± 10.0	28.58 ± 8.7	414.84 ± 22.26	240.53 ± 18.54
(i)		<10		<7		30.67 ± 11.76
(f)		31.01 ± 7.48		9.4 ± 7.5		137.45 ± 15.34
HR 1099 (r)	587.78 ± 33.17	458.55 ± 37.14	470.08 ± 35.0	372.84 ± 31.71	4421.27 ± 72.63	1231.66 ± 45.61
(i)		90.74 ± 34.94		110.08 ± 27.41		191.75 ± 34.16
(f)		262.68 ± 31.14		188.34 ± 27.24		727.60 ± 39.44

4.3.1. Si XIII and Mg XI triplets

The Si XIII and the Mg XI triplets at 6.7 Å and 9.2 Å are formed at temperatures of 7 MK and 6.8 MK and are density sensitive at densities $\log(n_{\rm e}) > 10^{12}$ cm^{-3}. In contrast to the HETGS with its larger effective areas and higher resolution, these triplets are not fully resolved in the LETGS spectra, but the blend can be modeled by a set of three partially overlapping lines with fixed wavelength differences. For example, the Si XIII triplet for Algol was modeled by Ness et al. (2002a) and a plot is shown there. As can be seen from Table 3 the Mg XI triplet is not detected for AD Leo and is very weak in UX Ari and YY Gem. Figure 2 demonstrates this procedure for the Mg XI triplet for Capella with our best fit. From this plot it can be seen that the line blend can be well modeled with the three lines for Mg XI. All our results quoted in this paper on the Si XIII and the Mg XI triplets have been obtained with such a de-blending procedure.

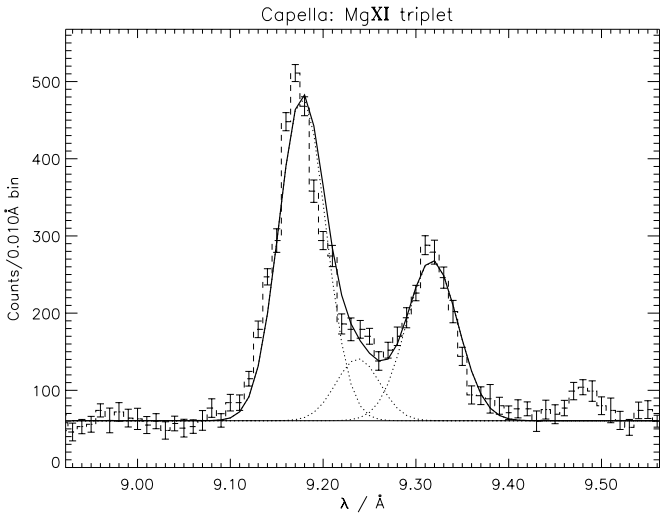

Fig. 2. Measured spectrum of the Mg XI triplet for Capella with the best fit.

4.3.2. Ne IX triplet

The analysis of the Ne IX triplet is complicated because of severe blending of the intercombination line with Fe XIX at 13.51 Å. An approach of still obtaining useful results is introduced for Algol by Ness et al. (2002a), where the G-ratio $(f + i)/r$ is fixed to 0.8 as is expected for a collision dominated plasma with a reasonable temperature. In this

Table 4. Modeling of contaminating Fe lines in the Ne IX triplet in comparison with the Fe XVII line at 15 Å. The last column contains the ratio of the hot 13.51 Å line with the cooler 15 Å line, corrected for effective areas and converted to energy fluxes.

λ/Å	13.51	13.65	13.79	13.83	15.01	(13.51)/(15.01)
$A_{\rm eff}$/cm^2	26.2	26.27	26.31	26.32	27.21	1.039
	Fe XIX/XXI	Fe XIX	Fe XIX	Fe XVII	Fe XVII	
Algol	585.68 ± 39.30	<29	134.69 ± 30.13	47.70 ± 28.39	1018.44 ± 38.93	0.66 ± 0,05
Capella	4046.6 ± 89.18	470.89 ± 49.98	2173.57 ± 73.68	1839.88 ± 70.43	23146.21 ± 161.52	0.20 ± 0.005
Procyon		22.56 ± 7.52			105.94 ± 13.81	
ϵ Eri	147.26 ± 20.81	<13	34.10 ± 14.24	80.25 ± 15.6	1188.05 ± 36.92	0.14 ± 0.02
UX Ari	195.87 ± 28.18	<20	51.58 ± 21.64	<30	383.02 ± 25.67	0.59 ± 0.09
AD Leo	59.49 ± 14.84	<20	46.61 ± 11.65	<20	300.18 ± 19.52	0.23 ± 0.06
YY Gem	91 ± 15.1	<16	22.4 ± 10.4	<20	234.29 ± 17.64	0.45 ± 0.08
HR 1099	593.43 ± 42	<30	218 ± 33.3	77.9 ± 30.65	1059.2 ± 41	0.65 ± 0.05

paper we follow a different, more empirical approach. In an HEG spectrum of Capella (Ness et al. 2002b) a total of 18 lines can be identified, which we combine – for the purposes of LETGS modeling – into a set of four contaminating lines (which are listed in Table 4). These contamination lines are due to Fe XVII and Fe XIX. With these seven lines, i.e., four lines from Fe XVII/XIX and the three Ne IX He-like triplet lines we calculate a best fit. The relative line positions as well as the line widths (σ = 0.0222 Å) are kept constant during the iteration. The fit results for HR 1099 and Capella are shown in Fig. 3. Obviously a good fit can be obtained with the wavelengths estimated from the Capella HEG spectrum for both stars. The two double peaks visible in the Capella spectrum appear in a different form in the HR 1099 spectrum. We attribute this difference to an anomalously high Ne abundance in HR 1099 (cf., e.g., Brinkman et al. 2001). In the spectrum of HR 1099 we additionally identified Ne X Ly$_{\alpha,\beta,\gamma,\text{ and }\delta}$ with 45.35 ± 0.74, 6.04 ± 0.34, 2.33 ± 0.27, and 1.96 ± 0.26 cts/ksec and for Capella with 20.65 ± 0.33, 2.69 ± 0.15, 1.04 ± 0.12, and 0.88 ± 0.12 cts/ksec, respectively. The count rates differ by a factor of more than two in favor of HR 1099 suggesting higher Ne abundances in HR 1099 compared to Capella. We consider temperature effects less important, at least not accounting for this large discrepancy.

As a cross check we compare the strengths of the contaminating line at 13.51 Å with the strong isolated Fe XVII line at 15 Å. In Table 4 we show the fit results for all contaminating lines and for the 15 Å line. In the last column we calculated the flux ratios of the 13.51 Å line and the 15 Å line. These ratios are plotted in Fig. 4 in comparison with the temperature dependent theoretical curve as calculated with MEKAL (Mewe et al. 1995) assuming the 13.51 Å line to consist of two Fe XIX lines at 13.504 Å and 13.52 Å. Under this assumption the ratio (13.51)/(15.01) must be temperature sensitive since Fe XIX is formed at higher temperatures than Fe XVII. From Fig. 4 we see a trend suggesting Algol, HR 1099, and UX Ari to contain the hottest plasma in our sample. This is consistent with our temperature measurements in Tables 5 to 7 as well as with the trend seen in Fig. 9. The ratios for the other stars seem also very

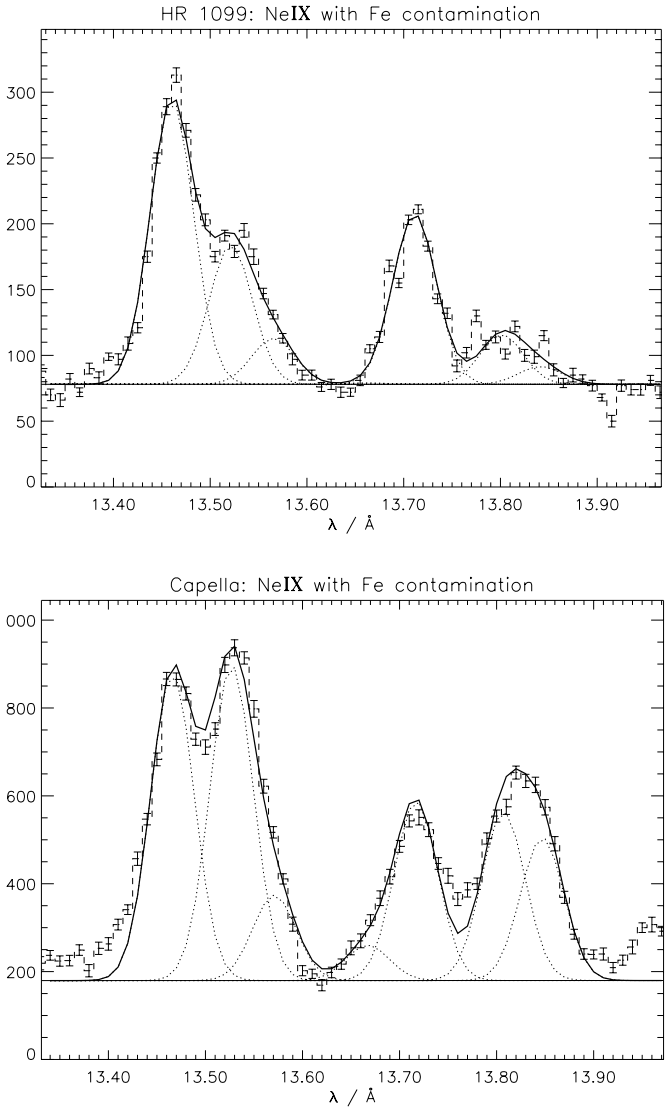

Fig. 3. Measured spectrum of the Ne IX triplet with Fe contamination for HR 1099 (top) and Capella (bottom) with the best fits using seven wavelength values (cf. Table 4) iterated only as a whole multiplet complex. The Gaussian line width is fixed to σ = 0.0222 Å for all lines.

Table 5. Results for O VII, N VI, and C V for the "cooler" stars Procyon and α Cen A and B. The errors are 1 σ errors. For each ion the measured He-like ratios $R = f/i$ and $G = (f+i)/r$, and the ratios Ly_α/r and $Ly_\alpha/He = Ly_\alpha/(r+i+f)$ are given. The derived $T(Ly_\alpha/r)$, $T(Ly_\alpha/He)$, and $T(G)$ and the densities $\log(n_e(f/i))$ are also given. $^1\log(n_e)$ denotes the densities accounting for ϕ/ϕ_c; the radiation terms ϕ/ϕ_c used for the density diagnostics were measured with IUE as described by, e.g., Ness et al. (2001a). Effective areas are taken from Deron Pease (Oct. 2000).

	Procyon	α Cen	
		A	B
HD	61421	128620	128621
t_{exp}/ksec	140.7	81.5	
$N_c = 3.4 \times 10^{10}$ cm^{-3}, $R_0 = 3.95$	**O** VII		
$T_m = 2.0$ MK	^{1} densities accounting for ϕ/ϕ_c		
f/i	3.22 ± 0.30	3.81 ± 1.06	5.6 ± 2.9
$(f+i)/r$	1.21 ± 0.08	1.0 ± 0.17	1.17 ± 0.17
Ly_α/r	0.67 ± 0.04	0.38 ± 0.07	0.64 ± 0.08
Ly_α/He	0.31 ± 0.03	0.19 ± 0.06	0.30 ± 0.08
T_{rad}/K	5410	4653	4181
ϕ/ϕ_c	0.01	0.01	0
$^1\log(n_e/cm^{-3})$	9.28 ± 0.4	8.96 ± 1.20	–
$\log(n_e/cm^{-3})$	9.89 ± 0.26	9.70 ± 0.58	–
$T(Ly_\alpha/r)$/MK	2.20 ± 0.03	1.93 ± 0.08	2.17 ± 0.07
$T(Ly_\alpha/He)$/MK	2.85 ± 0.04	1.68 ± 0.10	1.83 ± 0.10
T(G)/MK	0.96 ± 0.25	1.67 ± 0.74	1.09 ± 0.56
$N_c = 5.27 \times 10^9$ cm^{-3}, $R_0 = 6.0$	**N** VI		
$T_m = 1.4$ MK	^{1} densities accounting for ϕ/ϕ_c		
f/i	1.33 ± 0.28	2.19 ± 0.86	2.09 ± 1.4
$(f+i)/r$	0.93 ± 0.16	1.43 ± 0.45	1.39 ± 0.66
Ly_α/r	0.94 ± 0.11	0.49 ± 0.17	1.45 ± 0.49
Ly_α/He	0.49 ± 0.12	0.20 ± 0.10	0.61 ± 0.47
T_{rad}/K	5780	4626	3994
ϕ/ϕ_c	1.58 ± 0.84	0.07	0.005
$^1\log(n_e/cm^{-3})$	9.96 ± 0.23	9.95 ± 0.30	9.99 ± 0.65
$\log(n_e/cm^{-3})$	10.27 ± 0.12	9.96 ± 0.30	10.00 ± 0.64
$T(Ly_\alpha/r)$/MK	1.09 ± 0.13	1.35 ± 0.09	1.79 ± 0.16
$T(Ly_\alpha/He)$/MK	1.41 ± 0.07	1.15 ± 0.09	1.43 ± 0.22
T(G)/MK	1.28 ± 0.46	<1.2	<1.8
$N_c = 6.7 \times 10^8$ cm^{-3}, $R_0 = 11.6$	**C** V		
$T_m = 1.0$ MK	^{1} densities accounting for ϕ/ϕ_c		
f/i	0.52 ± 0.13	2.07 ± 2.	3.24 ± 2.86
$(f+i)/r$	1.39 ± 0.24	0.75 ± 0.48	1.56 ± 0.85
Ly_α/r	1.78 ± 0.17	1.56 ± 0.37	2.01 ± 0.60
Ly_α/He	0.75 ± 0.19	0.89 ± 0.89	0.79 ± 0.73
T_{rad}/K	5532	4864	4124
ϕ/ϕ_c	26.67 ± 9.3	5.7	0.6
$^1\log(n_e/cm^{-3})$	<8.92	<11.04	9.13 ± 1.16
$\log(n_e/cm^{-3})$	10.16 ± 0.12	9.50 ± 1.56	9.24 ± 1.05
$T(Ly_\alpha/r)$/MK	1.18 ± 0.03	1.14 ± 0.07	1.22 ± 0.10
$T(Ly_\alpha/He)$/MK	0.95 ± 0.54	1.00 ± 0.86	0.96 ± 0.17
T(G)/MK	<0.4	1.17 ± 0.8	<1.3

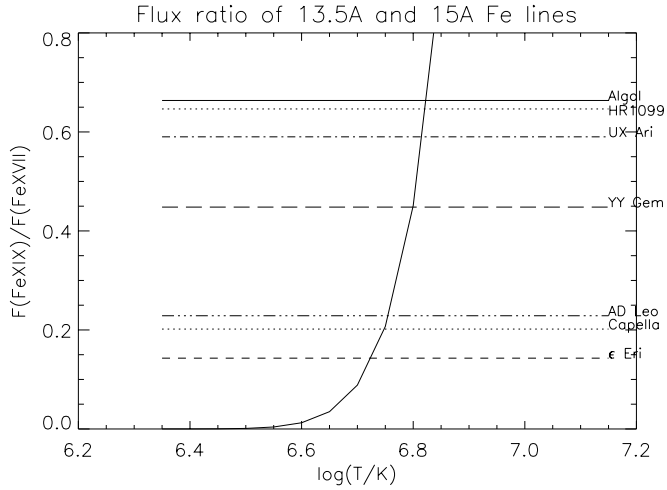

Fig. 4. Comparison of flux ratios derived from the 13.51 Å line (which contaminates the Ne IX intercombination line) and the strong Fe XVII line at 15 Å with the MEKAL ratio (solid curve). The theoretical 13.52 Å flux is derived assuming the MEKAL lines at 13.504 Å and 13.52 Å to contribute with their individual fluxes.

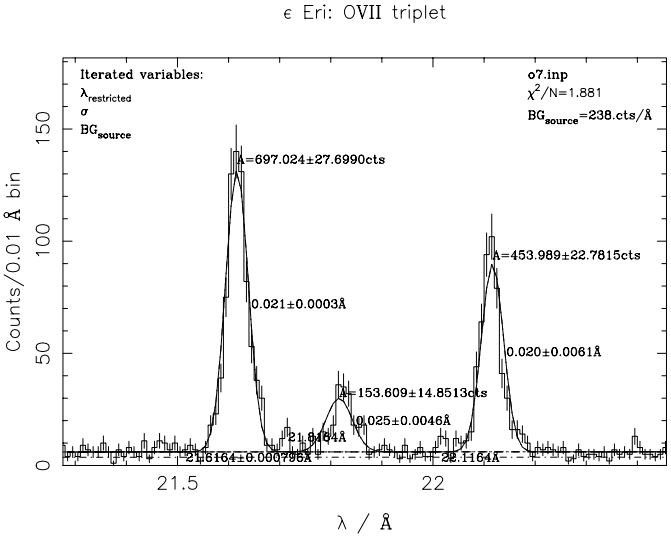

Fig. 5. Measurement of the O VII triplet for ϵ Eri (105 ksec).

reasonable. We finally point out that the G-ratios derived from our Ne measurements are all consistent with the expected value of 0.8, which again demonstrates internal self-consistency of our procedure.

Another problem with Ne is the blending of H-like Ne X at 12.14 Å with Fe XVI/Fe XVII (λ = 12.134 Å). The contamination with the Fe lines is most critical at temperatures less than 4 MK, and can be neglected at temperatures higher than 6 MK.

4.3.3. O VII triplet

The most prominent He-like triplet is the O VII triplet which is detected in all stars. In Fig. 5 we show the region around the O VII triplet for ϵ Eri; the resonance line, the intercombination line, and the forbidden line are all clearly detected above the

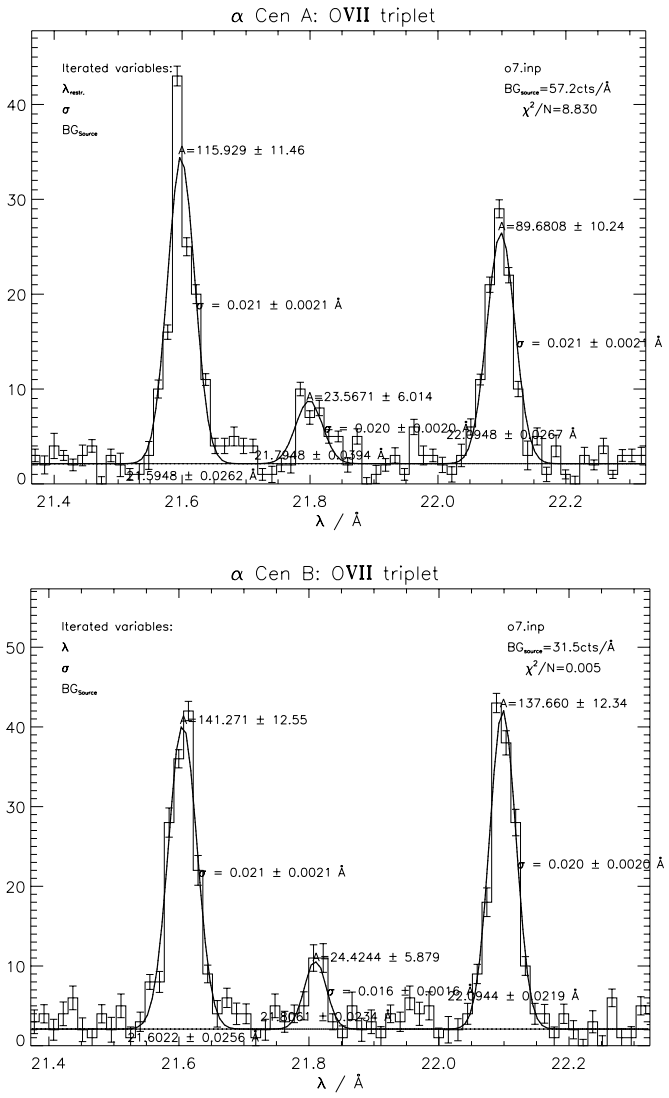

Fig. 6. Measurement of the O VII triplet for α Cen A (top) and B (bottom) (81.5 ksec).

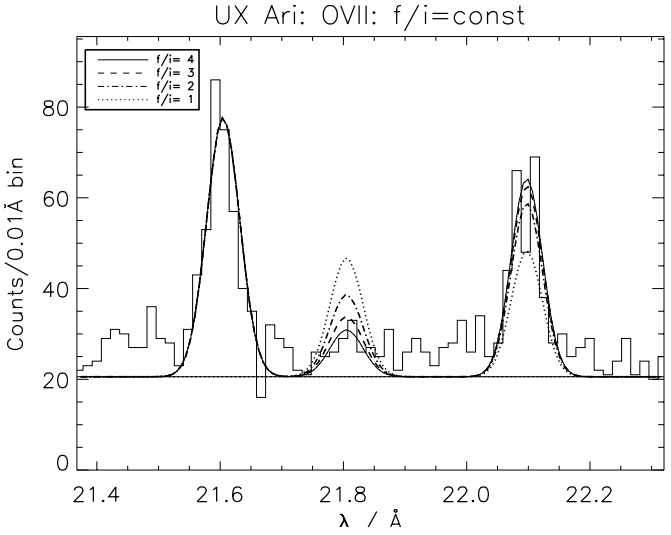

Fig. 7. Measured spectrum of the O VII triplet for UX Ari with best fits constrained to satisfy f/i = 4, 3, 2, and 1.

weak continuum. A weak line at 21.7 Å may be present, but it does not compromise the measurement of the O VII line fluxes. For the f/i-ratio for ϵ Eri we find a value of 2.96 ± 0.32, which is not consistent with the low density limit of 3.95.

In Fig. 6 we plot the O VII triplets for α Cen A and B, which can easily be spectrally resolved because of the superb angular resolution of the *Chandra* mirrors. These spectra have lower SNR than the ϵ Eri spectrum and we measure $f/i = 3.81 \pm 1.06$ and $f/i = 5.6 \pm 2.9$, i.e., numbers which are fully consistent with the low density limit.

In Fig. 7 we show the O VII triplet for UX Ari. The corona of UX Ari is much hotter than that of ϵ Eri and α Cen A and B. Therefore the continuum is much higher so that the weakest line of the O VII triplet, the intercombination line, is not detected, while the resonance line and the forbidden line are. This implies that UX Ari shows different properties compared to Algol where intercombination and forbidden line have approximately the same strength (cf. Ness et al. 2002a). To better illustrate the observational situation we plot in Fig. 7 the recorded UX Ari LETGS spectrum with f/i-ratios of 4, 3, 2, and 1 superimposed. Clearly, the LETGS measurements are consistent with the low density limit, but f/i-ratios as low as $f/i \sim 2$ cannot be excluded.

4.3.4. N VI triplet

The N VI triplet at 28.8, 29.1, and 29.5 Å has been detected in all stars but YY Gem (cf. Stelzer et al. 2002) and HR 1099. In all cases do we find f/i-values considerably below the low density limit $R_{0,\mathrm{N}} = 6.0$, the largest measurement being 2.19 ± 0.86 for α Cen A and the smallest one being 0.21 ± 0.09 for Algol. The interpretation of the N VI triplet must take possible radiation effects into consideration (cf. Sect. 5.1). However, for cool stars such as AD Leo, YY Gem, and ϵ Eri these radiation effects are very small and the low f/i-ratio can unambiguously be attributed to a density effect.

4.3.5. C V triplet

The analysis of the C V triplet at 41 Å is intimately connected with measuring the Ne IX triplet and the Fe contamination, which appears superimposed on C V in third order. Fortunately, for the cool coronae of α Cen A and B and Procyon emission from Ne IX and Fe XVII ions is either weak or absent in first order (and particularly in third order which is damped by a factor ≈20), so that C V can be directly measured. For those stars emission from the C V triplet is detected; the data for Procyon are discussed by Ness et al. (2001a), for both components of α Cen the SNR is so low that the intercombination line is only marginally detected at best, while the resonance and forbidden lines are. Thus detailed density diagnostics are hardly called for. For all other stars the forbidden line of C V is severely contaminated by third order lines at 13.8 Å. This is a specific disadvantage of the LETGS, however, no other instrument can measure the C V triplet. Since the first order signal is also recorded by the same instrument, it is still

possible to model the C v triplet taking the third order contamination explicitly into account. This was demonstrated by Ness et al. (2001a) for Capella, however, such a procedure requires high SNR data, which are unfortunately available only for Capella. Since in addition in the active stars Algol, UX Ari, and HR 1099 the carbon lines are absent or weak (cf. Schmitt & Ness 2002), we therefore refrained from carrying out a similar modeling procedure for the other sample stars.

5. Results

In Tables 5 to 7 we provide a summary of the plasma diagnostic results of our analysis for the He-like ions Si XIII, Mg XI, Ne IX, O VII, N VI, and C V. Some ions are not detected as, e.g., C V is not detected in the hot stars Algol and UX Ari, or Si XIII is not detected in the cool coronae of Procyon and α Cen A and B. The ratio of H-like to He-like, Ly_α/r, can not always be measured, since the He-like triplet cannot always be fully resolved for silicon and magnesium. For those cases the ratio $\mathrm{Ly}_\alpha/(r+i+f) = \mathrm{Ly}_\alpha/\mathrm{He}$ is also given. In the following we describe how temperatures and densities are derived.

5.1. Influence of radiation fields

Our sample contains stars of type B to M, which differ dramatically in their photospheric radiation fields. Specific attention must therefore be paid to the presence of such fields which are different for the different He-like lines as well as in our sample stars. For the stars with hotter photospheric temperatures, the effects of radiation fields on the low-Z ions cannot be neglected (e.g., Ness et al. 2001b, 2001c). In our sample the stars Procyon, Capella, and Algol are of particular interest in that respect. For Procyon and Capella we use the results obtained by Ness et al. (2001a) and for Algol the results obtained by Ness et al. (2002a). In the case of Algol we note that with the effects of the radiation field, which originates from the companion B star, we assume a worst case scenario with the X-ray corona fully immersed in the B-star's radiation field; Ness et al. (2001b) discuss the possible geometrical configurations of the binary at the time of the observation. For the K stars (cf. Table 1) the effects of radiation fields can be neglected. For α Cen A and B we measured the radiation fields with IUE, corresponding to Ness et al. (2001a), and found that the radiation affects only the C v triplet (cf. Table 5 and Ness et al. 2001c). All the results of the radiation fields measured with IUE are illustrated in Fig. 8, where the influence is given in terms of corrected low density limits.

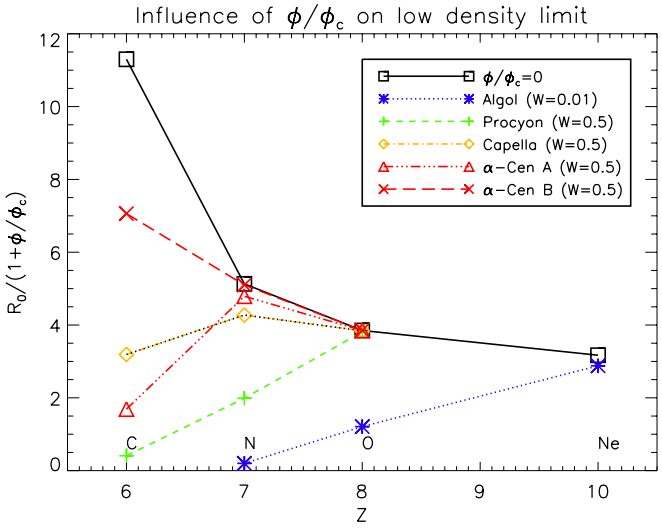

Fig. 8. Influence of different radiation fields on the low-density limit restricting the density diagnostics. W is the dilution factor applied accounting for the geometry of the stars. Plotted is the expected f/i ratio for the case $n_e = 0$ (cf. Eq. (1)) versus atomic number Z.

5.2. Densities

The results of our measurements of the ratio of forbidden and intercombination lines in the He-like triplets of Si, Mg, Ne, O, N, and C are listed in Tables 5 to 7. In our analysis we attribute all measured counts to the respective intercombintion and forbidden lines; possible contamination by other coincidental lines or dielectronic satellite lines will be discussed in Sect. 6. For the purpose of discussion we assume the low-density case and ask to what extent and at what confidence we can exclude the low-density case on the basis of our LETGS measurements. Specifically, we consider only those cases where the low-density limit can be excluded at least on the "$2\,\sigma$" level. For Si the only measurement indicating deviations from the low-density limit are those for AD Leo. The Si triplet is clearly broadened, yet the overall signal is rather low. We also modeled the Si XIII triplet with the constraint of $f/i = 2.6$, i.e., the low density limit, and found this fit only slightly worse. We therefore conclude that any claim for a deviation of the Si XIII triplet from the low-density limit needs confirmation from an MEG or HEG measurement. For the Mg triplet no deviation from the low-density limit above the $2\,\sigma$ level can be observed. For neon the only two stars with significant deviations from the low density limit are UX Ari and Capella. In the latter case our measurement, i.e., 2.08 ± 0.14, deviates significantly from the low density limit of 3.5. This is puzzling since the corresponding measurement for the O VII triplet is consistent with the low density limit. From the higher resolution *Chandra* MEG measurements of Ne IX Ayres et al. (2001) find $f/i = 2.9 \pm 0.5$ for Ne IX and 2.6 ± 0.3 for O VII. From an apparently different *Chandra* MEG spectrum of Capella Phillips et al. (2001) find an f/i-ratio of 2.64 ± 0.56 for O VII in agreement with the values reported by Ayres et al. (2001), while for Ne IX these authors argue that the agreement between the *Chandra* data and a low-density synthetic model spectrum is reasonable. Neither number is consistent with our measurements, we note, however, that the MEG measurements of Si, Mg, Ne, and O in HR 1099 analyzed by Ayres et al. (2001) are all consistent with our results. Also, Ness et al. (2002b) find a Ne IX f/i ratio for Capella consistent with our results using all HEG measurements available for Capella. While our O VII-ratio for Capella is consistent with the XMM-RGS measurement for Capella reported by Audard et al. (2001b), a lower f/i ratio is found only with the MEG measurements. This discrepancy is only found

Table 6. Results for O VII, N VI, and C V for the "hotter" stars corresponding to Table 5.

	Algol	Capella	ϵ Eri	UX Ari	AD Leo	YY Gem	HR 1099
HD	19356	34029	22049	21242	GL388	60179C	22468
t_{exp}/ksec	81.4	218.5	105.3	112.76	48.5	59	97.5
$N_c = 3.4 \times 10^{10}$ cm^{-3}, $R_0 = 3.95$				**O VII**			
$T_m = 2.0$ MK	[1] densities accounting for ϕ/ϕ_c						
f/i	0.96 ± 0.2	3.92 ± 0.25	2.96 ± 0.32	>4	3.22 ± 0.62	2.29 ± 0.5	2.22 ± 0.41
$(f+i)/r$	0.98 ± 0.17	0.9 ± 0.03	0.86 ± 0.06	0.7 ± 0.14	0.86 ± 0.11	0.88 ± 0.14	0.80 ± 0.10
Ly$_\alpha/r$	8.03 ± 0.71	3.49 ± 0.07	2.12 ± 0.10	10.05 ± 0.93	3.43 ± 0.1	3.67 ± 0.32	8.67 ± 0.53
T_{rad}/K	12710	5030	0	0	0	0	0
ϕ/ϕ_c	2.18 ± 0.29	0.003	0	0	0	0	0
[1]log(n_e/cm^{-3})	10.5 ± 0.62	<9.38	10.03 ± 0.23	–	9.89 ± 0.9	10.39 ± 0.24	10.42 ± 0.19
log(n_e/cm^{-3})	11.04 ± 0.12	8.36 ± 1.04	9.10 ± 1.08	–	9.89 ± 0.9	10.39 ± 0.24	10.42 ± 0.19
T(Ly$_\alpha/r$)/MK	4.81 ± 0.18	3.54 ± 0.02	3.00 ± 0.04	5.27 ± 0.20	3.52 ± 0.08	3.6 ± 0.1	4.98 ± 0.12
T(G)/MK	1.72 ± 0.74	2.0 ± 0.13	2.22 ± 0.30	3.14 ± 0.83	2.2 ± 0.6	2.15 ± 0.71	2.52 ± 0.64
$N_c = 5.2 \times 10^9$ cm^{-3}, $R_0 = 6.0$				**N VI**			
$T_m = 1.4$ MK	[1] densities accounting for ϕ/ϕ_c						
f/i	0.21 ± 0.09	1.78 ± 0.25	1.15 ± 0.55	1.44 ± 0.86	1.07 ± 0.61	–	–
$(f+i)/r$	1.66 ± 0.39	1.33 ± 0.15	1.00 ± 0.39	0.69 ± 0.31	1.48 ± 0.73	–	–
Ly$_\alpha/r$	8.37 ± 1.28	4.91 ± 0.34	3.78 ± 0.79	6.68 ± 1.10	5.48 ± 1.62	–	–
Ly$_\alpha$/He	3.19 ± 1.38	2.14 ± 0.33	1.91 ± 0.99	3.92 ± 2.44	2.23 ± 1.44	–	–
T_{rad}/K	12060	4980	0	0	0	0	0
ϕ/ϕ_c	24.74 ± 2.41	0.2 ± 0.1	0	0	0	0	0
[1]log(n_e/cm^{-3})	10.20 ± 0.93	9.86 ± 0.12	10.35 ± 0.33	10.23 ± 0.47	10.39 ± 0.42	–	–
log(n_e/cm^{-3})	11.16 ± 0.23	10.09 ± 0.09	10.35 ± 0.32	10.23 ± 0.47	10.39 ± 0.42	–	–
T(Ly$_\alpha/r$)/MK	3.42 ± 0.23	2.73 ± 0.08	2.47 ± 0.18	3.08 ± 0.21	2.86 ± 0.33	–	–
T(Ly$_\alpha$/He)/MK	2.32 ± 0.34	2.02 ± 0.10	1.95 ± 0.30	2.51 ± 0.53	2.05 ± 0.4	–	–
T(G)/MK	<0.7	0.46 ± 0.28	<2.4	2.1 ± 0.9	<2	–	–
$N_c = 6.7 \times 10^8$ cm^{-3}, $R_0 = 11.6$				**C V**			
$T_m = 1.0$ MK	[1] densities accounting for ϕ/ϕ_c						
f/i	–	1.60 ± 0.37	*contaminated*	*contaminated*	–	–	–
$(f+i)/r$	–	0.91 ± 0.15	–	–	–	–	–
Ly$_\alpha/r$	–	2.55 ± 0.17	2.93 ± 0.58	2.87 ± 0.50	3.34 ± 0.93	–	–
T_{rad}/K	–	4585	–	–	–	–	–
ϕ/ϕ_c	–	2.54 ± 0.86	–	–	–	–	–
[1]log(n_e/cm^{-3})	–	9.42 ± 0.21	–	–	–	–	–
log(n_e/cm^{-3})	–	9.63 ± 0.12	–	–	–	–	–
T(Ly$_\alpha/r$)/MK	–	1.32 ± 0.03	1.38 ± 0.08	1.37 ± 0.08	1.44 ± 0.13	–	–
T(G)/MK	–	0.85 ± 0.3	–	–	–	–	–

for Capella but not for HR 1099. Concerning the discrepancy with Ne IX for Capella we point out that the blending problems are more severe with the LETGS than with the MEG, such that the higher f/i-ratios for Ne IX measured with the MEG seem to be more reliable. However, the HEG has a better resolution than the MEG, such that the spectra analysed by Ness et al. (2002b) should be most reliable. Obviously, the best data are available for the oxygen triplet; for Algol, Procyon, YY Gem, ϵ Eri, and HR 1099 do we find significant deviations from the low-density limit and interpret those results in Sect. 6.

Table 7. Results for Si XIII, Mg XI, and Ne IX corresponding to Table 5. The errors are 1 σ errors including correlated errors in line blends.

	Algol	Capella	ϵ Eri	UX Ari	AD Leo	YY Gem	HR 1099	Procyon
HD	19356	34029	22049	21242	Gl388	60179C	22468	61412
t_{exp}/ksec	81.4	218.5	105.3	112.76	48.5	59	97.5	140.7
$N_c = 3.9 \times 10^{13}$ cm^{-3}, $R_0 = 2.67$					**Si XIII**			
$T_m = 10.0$ MK								
f/i	3.66 ± 1.45	4.41 ± 0.91	–	3.02 ± 2.54	1.32 ± 0.55	–	2.91 ± 1.17	–
$(f+i)/r$	0.83 ± 0.15	0.67 ± 0.05	0.82 ± 0.36	0.61 ± 0.22	0.99 ± 0.32	–	0.78 ± 0.16	–
Ly$_\alpha/r$	1.54 ± 0.14	0.31 ± 0.02	0.21 ± 0.14	1.11 ± 0.16	0.72 ± 0.17	0.99 ± 0.22	1.44 ± 0.14	–
Ly$_\alpha$/He	0.84 ± 0.34	0.18 ± 0.04	–	0.69 ± 0.59	0.36 ± 0.17	–	0.82 ± 0.34	–
log(n_e/cm^{-3})	<12.9	<12.1	<14.25	<14.25	13.6 ± 0.4	–	<13.32	–
T(Ly$_\alpha/r$)/MK	14.61 ± 0.49	8.80 ± 0.14	8.0 ± 1.1	12.96 ± 0.6	11.26 ± 0.77	12.5 ± 0.9	14.28 ± 0.48	–
T(Ly$_\alpha$/He)/MK	11.80 ± 1.41	7.75 ± 0.37	–	11.1 ± 2.54	9.18 ± 1.09	–	11.68 ± 1.46	–
T(G)/MK	6.2 ± 3.0	–	–	11.4 ± 5.3	<9	–	7.1 ± 4.1	–
$N_c = 6.2 \times 10^{12}$ cm^{-3}, $R_0 = 2.6$					**Mg XI**			
$T_m = 6.3$ MK								
f/i	–	3.04 ± 0.53	1.59 ± 0.63	–	–	–	1.72 ± 0.50	–
$(f+i)/r$	–	0.74 ± 0.04	1.06 ± 0.33	–	–	–	0.81 ± 0.16	–
Ly$_\alpha/r$	2.4 ± 0.31	0.59 ± 0.02	0.61 ± 0.17	3.24 ± 1.27	–	1.46 ± 0.55	1.18 ± 0.13	–
Ly$_\alpha$/He	1.40 ± 0.60	0.34 ± 0.03	0.30 ± 0.14	–	–	–	0.65 ± 0.2	–
log(n_e/cm^{-3})	–	<11.35	12.6 ± 0.6	–	–	–	12.5 ± 0.5	–
T(Ly$_\alpha/r$)/MK	10.43 ± 0.51	6.63 ± 0.07	6.69 ± 0.49	11.7 ± 1.7	–	8.74 ± 1.03	8.14 ± 0.28	–
T(Ly$_\alpha$/He)/MK	8.62 ± 1.14	5.76 ± 0.12	5.60 ± 0.55	–	–	–	6.82 ± 0.55	–
T(G)/MK	–	5.8 ± 0.6	–	–	–	–	4.6 ± 2.96	–
$N_c = 5.9 \times 10^{11}$ cm^{-3}, $R_0 = 3.5$					**Ne IX**			
$T_m = 10.0$ MK								
f/i	4.31 ± 1.69	2.08 ± 0.14	2.97 ± 0.49	2.47 ± 0.37	5.38 ± 2.13	4.47 ± 1.79	3.79 ± 0.7	2.58 ± 1.41
$(f+i)/r$	0.68 ± 0.11	0.86 ± 0.04	0.82 ± 0.08	0.75 ± 0.07	0.71 ± 0.11	0.70 ± 0.12	0.74 ± 0.07	0.72 ± 0.25
Ly$_\alpha/r$	4.56 ± 0.28	1.90 ± 0.05	0.99 ± 0.07	4.04 ± 0.18	1.71 ± 0.15	2.0 ± 0.19	4.17 ± 0.17	0.19 ± 0.09
Ly$_\alpha$/He	2.74 ± 1.09	1.03 ± 0.07	0.55 ± 0.10	2.33 ± 0.37	1.01 ± 0.41	1.19 ± 0.49	2.41 ± 0.46	0.11 ± 0.08
ϕ/ϕ_c	0.1 ± 0.03	0	0	0	0	0	0	0
log(n_e/cm^{-3})	<11.3	11.61 ± 0.07	11.02 ± 1.15	11.39 ± 0.26	<10.65	<11.25	<10.91	11.32 ± 0.75
T(Ly$_\alpha/r$)/MK	7.66 ± 0.21	5.46 ± 0.05	4.44 ± 0.09	7.28 ± 0.13	5.27 ± 0.16	5.58 ± 0.17	7.37 ± 0.12	2.95 ± 0.26
T(Ly$_\alpha$/He)/MK	6.26 ± 0.88	4.49 ± 0.08	3.67 ± 0.18	5.87 ± 0.34	4.47 ± 0.49	4.68 ± 0.55	5.94 ± 0.42	2.67 ± 0.28
T(G)/MK	4.96 ± 1.57	2.7 ± 0.4	3.17 ± 0.96	4.1 ± 0.9	4.5 ± 1.6	4.7 ± 1.8	4.09 ± 0.85	4.3 ± 4.0

For the nitrogen triplet we find deviations from the low density limit for all stars where sensitive measurements could be made; note that for HR 1099 and YY Gem no clear detections of the N triplet are available. Our discussion in Sect. 5.1 indicates that for Algol and Procyon the low f/i-ratios can be attributed to the radiation field alone, in all other sample stars we must attribute the low f/i-ratios to high densities. As to the C V triplet, most of the LETGS data has very low SNR. The data for Procyon and α Cen A and B cannot be reconciled with the low-density limit and neither those for Capella (cf. Ness et al. 2001a), where the higher order contamination can be well modelled. In all other cases we can make no particularly sensitive statements except noting that in AD Leo and possibly YY Gem the C V resonance line is detected and far higher SNR is required for any definite conclusions.

5.3. X-ray luminosities and temperatures

As already discussed in Sect. 4.2 and listed in Table 1 we directly measured X-ray luminosities by evaluating the total energy flux from all photons recorded in a given wavelength bin and summing up. We note in passing that this procedure underestimates the true energy flux since photons from higher dispersion orders are treated incorrectly, however, the overall error introduced by this is rather small. In Tables 2 and 3 we list the Ly$_\alpha$-lines and the resonance lines of the He-like ions. Oxygen Ly$_\alpha$ and the oxygen He-like resonance lines are detected for all our sample stars, while the corresponding lines for nitrogen and neon are detected for almost all stars in our sample. The measured X-ray luminosities L_X range from $\approx 10^{27}$ up to 10^{32} erg/s while the measured line ratios between the Ly$_\alpha$ and the He-like resonance line range from values below unity

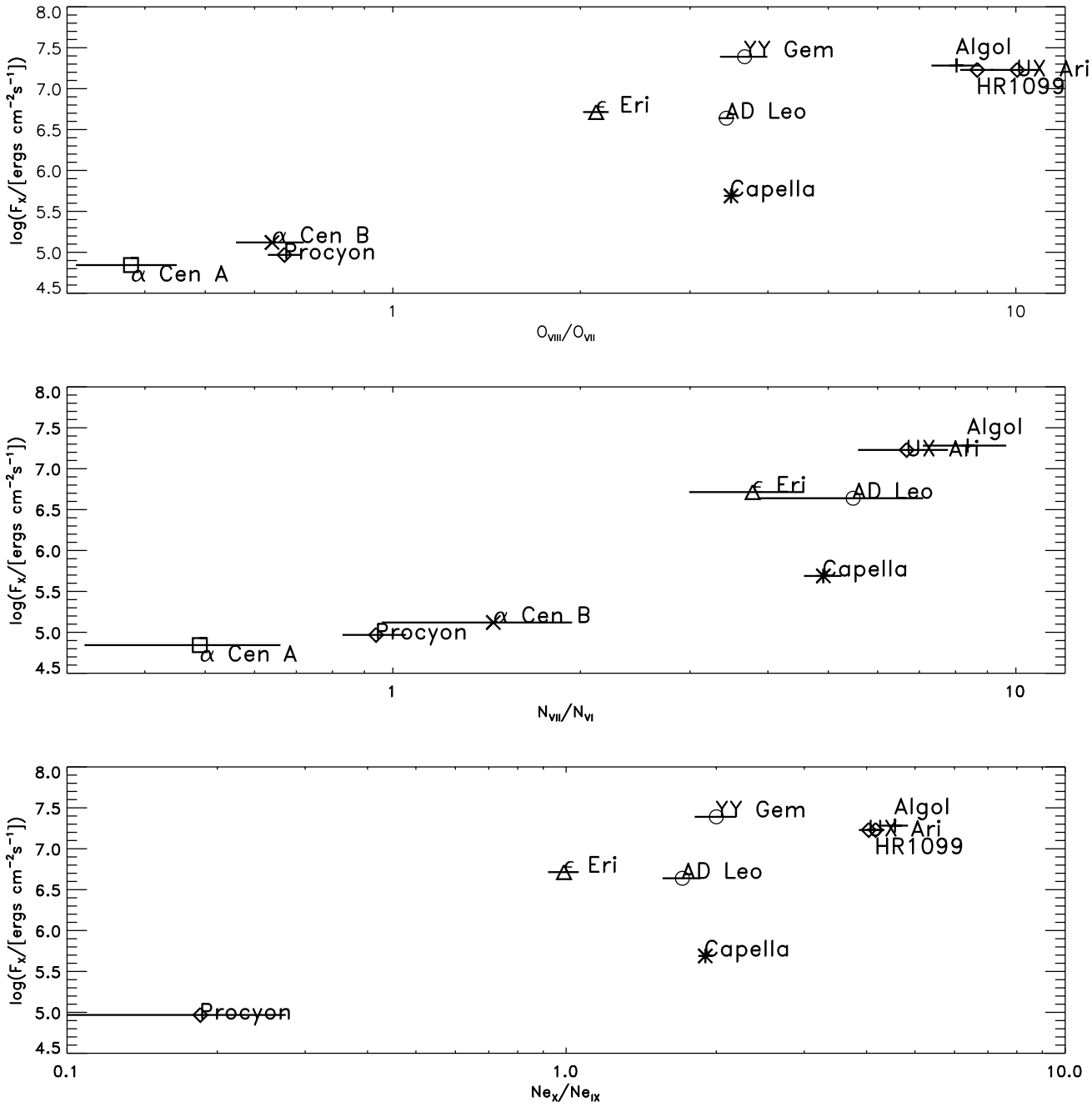

Fig. 9. Relation between line ratio Ly$_\alpha$/He-like and surface flux $F_X = L_X/4\pi R_\star^2$, with the stellar radii $R_\star$ in cgs units, for O VIII/O VII (top panel), N VII/N VI (middle panel), and Ne X/Ne IX (bottom panel).

for the inactive stars Procyon and α Cen A and B up to 10 for the most luminous stars Algol, UX Ari, and HR 1099. A similar trend is found when the ratios of the nitrogen Ly$_\alpha$ line and the He-like resonance line as well as the corresponding Ne ratios are considered. In Fig. 9 we plot the mean X-ray surface flux F_X, calculated as $L_X/4\pi R_\star^2$ with the stellar radii $R_\star$ taken from Table 1, for the line ratios O VIII/O VII, N VII/N VI, and Ne X/Ne IX. We refrain from carrying out a formal correlation analysis, but point out that larger mean X-ray surface fluxes tend to go together with larger line ratios between the Ly$_\alpha$ lines and the He-like resonance lines (cf. Fig. 9). For each atomic species the ratio between the Ly$_\alpha$ and He-like resonance line is a monotonic function of temperature. Larger line ratios therefore imply larger temperatures in the sense that the temperatures are weighted with the corresponding emission measures. Different atomic species are sensitive to emission measure in different temperature ranges and therefore represent different "effective" temperatures. Therefore Fig. 9 demonstrates a temperature-activity relationship. Such relationships between plasma temperature and X-ray luminosity are not entirely new (e.g., Schrijver et al. 1984; Schmitt et al. 1990), but measuring these line ratios as an indicator of temperature is new. The measured line ratios can also be directly converted into temperature if an isothermal plasma is assumed.

We computed temperatures by, first, comparing the measured line ratio of Ly_α lines with the recombination line of the corresponding He-like ions with a temperature dependent theoretical ratio taken from Mewe et al. (1985); alternatively we can use the total triplet emission for those cases in which the triplet is not fully resolved. An alternative way consists of using the He-like G ratio, $G = (f+i)/r$. In our analysis we compare the measured G ratios with the tables from Porquet et al. (2001), and interpolate quadratically. We always assume low densities, and point out that the temperature is not very sensitive to different densities. The temperatures derived in this fashion are quoted in Tables 5 to 7. Inspection of Tables 5 to 7 shows first that the temperatures derived with the two methods do not agree with the temperatures derived from the G-ratio in general being smaller than those derived from the Ly_α lines, and second, that different ions result in different temperatures, thus demonstrating that more than one temperature component must be present. We emphasize in this context that the above conclusions are independent of the elemental abundances since we use only ratios of the same species.

We also point out that the different stars "cluster" in certain regions of the F_X vs. Ly_α/r-ratio plane. This "clustering" is best apparent for oxygen where most measurements are available. The inactive stars α Cen A and B and Procyon form one group with $\log F_X \approx 5$ and O VIII/O VII ≈ 0.5. The active late-type dwarfs AD Leo, YY Gem, and ϵ Eri form another group with $\log F_X \approx 7$ and O VIII/O VII ≈ 3, the very active giants HR 1099, UX Ari, and Algol a third one with $\log F_X \approx 7.5$ and O VIII/O VII ≈ 9; the RS CVn-like binary Capella appears low in these diagrams because of the large radii (cf. Table 1), which lead to low mean X-ray surface fluxes. Whether or not this grouping represents a physical effect or is merely due to chance is difficult to tell in view of the sample of stars available. More observations covering a different variety of stars are clearly required.

5.4. Correlation between density and surface flux

In Fig. 10 we plot the f/i-ratios versus the X-ray surface flux F_X for N VI and O VII. For a graphical comparison between the densities in the stars we use the measured f/i ratios instead of densities, because the conversion of f/i into densities requires atomic data, which might be ambiguous, while the f/i ratios represent the original measurements. In order to give an impression of the corresponding densities we give the n_e scale on top of the graphs using the atomic data listed in Tables 5 to 7. Unfortunately the errors on f/i and hence density are still quite large, and for a number of stars, most notably α Cen A and B, no sensitive statements can be made. Nevertheless there appears to be a trend that smaller f/i-ratios (and hence high density) go together with higher density and (from Fig. 9) with higher temperature. We note in particular that UX Ari may in fact have a rather high density, and the density for Algol may in fact be too high since radiation effects are bound to play some role unless a very specific viewing geometry is assumed. It would be extremely interesting to construct diagrams such as shown in Fig. 10 for Ne, Mg, and Si, but this is not possible from the available LETGS data.

6. Conclusions

With the data from the new generation of X-ray telescopes we can measure He-like triplets for a wide range of temperatures and for stars other than the Sun. In our conclusions we consider only the cases as significant where deviations from the low-density limit are at least $2\,\sigma$. We point out that in all our stars the intercombination line is the weakest line (except for Algol), such that under exposed spectra suffer the most from large errors in the intercombination line leading to large uncertainties in the f/i ratios.

The theory of He-like triplets makes specific predictions for the ratio $(f+i)/r$, which for collisional dominated plasmas is near unity with some temperature dependence and for the density-dependent f/i-ratio. For the "hot" ions (neon, magnesium, silicon) the measured $(f+i)/r$-ratios are near but below unity, the same applies for the "cool" ions (carbon, nitrogen, and oxygen) for the "hot", i.e., active stars. For the less active stars (i.e., Procyon, α Cen A and B) the $(f+i)/r$-ratios are somewhat larger, so we conclude that our measurements are consistent with theoretical expectations, but unfortunately the accuracy of the measurements is such that temperature determinations with the help of the $(f+i)/r$-ratios are in many cases not possible.

As to densities, an inspection of Table 7 shows that for the elements neon, magnesium, and silicon no particularly convincing examples of density sensitive line ratios were found. Most measurements are consistent with the low-density limit and with the exception of Capella all "deviations" from the low-density limit are found only in one element at a significance between two and three σ. We thus conclude that for none of our sample stars the magnesium and silicon He-like triplets deviate from the low-density limit. For Capella we derive a neon f/i-ratio of 2.08 ± 0.14, significantly below the low-density limit. Interestingly, this value is confirmed by higher resolution measurements with the *Chandra* HEG (cf. Ness et al. 2002b). Note, however, that the intercombination line might be blended, which cannot be resolved with the HEG, such that the Ne measurements do not necessarily imply high densities.

Clearly, the best (in terms of signal-to-noise and spectral resolution) measurements are available for oxygen. For all ten stars the He-like resonance and forbidden lines were detected. The intercombination line, which is the weakest triplet line in a plasma with low to intermediate density, was detected for nine stars. In four cases (i.e., Algol, ϵ Eri, YY Gem, and HR 1099) do we find significant deviations from the expected low-density limit, in one case (Procyon) the measured f/i-ratio is within 2-3 σ from the low density limit. For the stars ϵ Eri, YY Gem, and HR 1099 we find f/i-ratios between 2.22–2.96, but the errors are so large that in principle those stars could have the same f/i-ratio. The by far lowest f/i-ratio is found for Algol, but in that particular case radiation fields can be important even for the oxygen triplet lines. In four cases (α Cen A and B, UX Ari, and AD Leo) the measurement errors are so large

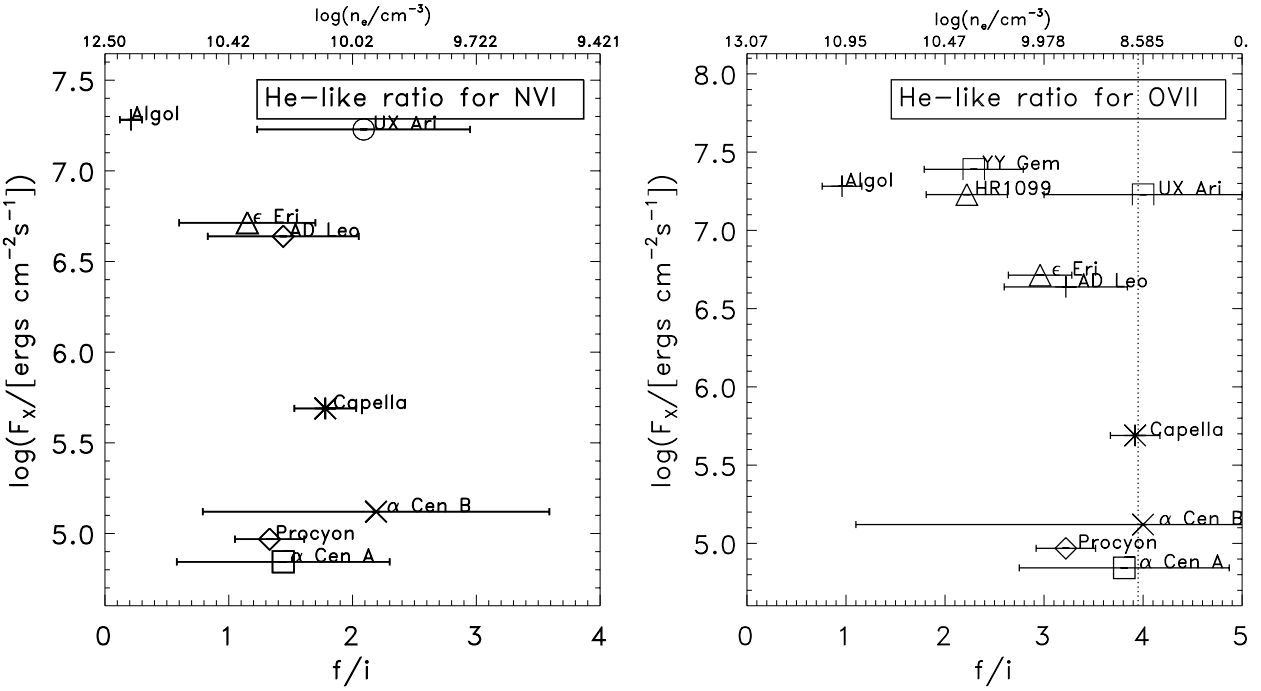

Fig. 10. f/i ratios for N VI (left panel) and for O VII (left panel) for the stars vs. X-ray surface flux (values listed in Table 1). 1 σ errors are given for f/i. On top of the graph are densities given assuming $\phi/\phi_c = 0$ and using the atomic parameters listed in Table 6.

that no meaningful conclusions can be drawn, while in one case (Capella) our measurement agrees perfectly with the low-density limit. This low-density for Capella is consistent with the XMM-Newton RGS results, but inconsistent with the measurements obtained with the *Chandra* MEG (cf., e.g., Canizares et al. 2000; Ayres et al. 2001; Phillips et al. 2001).

For our analysis we attribute all measured line counts to the expected He-like lines, which may be contaminated by coincidental lines or by dielectronic satellite lines. Such effects can be checked in each individual case. Specfically in the case of Procyon inspection of the MEKAL tables (Mewe et al. 1995) shows that a contribution from dielectronic satellite lines originating from O VI to the measured line flux of the intercombination line of O VII on the level of 10% can easily be accomplished. In this case the measured f/i ratio can well be consistent with the low-density limit. For the hotter coronae our measurement errors are larger and further the contribution from dielectronic satellite lines is weaker. Therefore low f/i ratios cannot be attributed to contamination of the intercombination line.

What implications can we deduce for the sizes of the underlying coronae? For the sake of argument, let us focus on the LETGS measurements of YY Gem. The available line ratios between Ly$_\alpha$ and He-like resonance lines can be described by a power-law differential emission measure distribution of the form $n_e^2 \frac{dV}{dT} dT = \xi(T) dT = \frac{EM_0}{T_0}(T/T_0)^\alpha dT$. With this functional form we find acceptable fits for the values $T_0 = 17$ MK and $\alpha = 0$. This results in values of 0.84, 1.69, 2.71, and 3.58 for the line ratios between the Ly$_\alpha$ and He-like resonance lines for Si, Mg, Ne, and O, respectively, which compare well (except for Ne) with our measurements of 0.99 ± 0.22, 1.46 ± 0.55, 2.0 ± 0.19, and 3.67 ± 0.32, respectively. Calculating the fluxes of the resonance, forbidden, and intercombination lines of the oxygen triplet with this emission measure distribution, we find for $(f + i)/r$ a value of 0.89, which must be compared to the measured value of 0.88 ± 0.14. The calculated f/i-ratio depends on the assumed pressure. If we assume a constant pressure scenario, we find an almost linear dependence of pressure and f/i-ratio, with the measured value of 2.29 corresponding to 17 dyne cm^{-2}. Unfortunately, the large errors in f/i make pressures as low as 10 dyne cm^{-2} and high as 28 dyne cm^{-2} also possible; at any rate, we can deduce a pressure of 20 ± 10 dyne cm^{-2} in the corona(e) of YY Gem. We note that this value is independent of the precise emission measure distribution adopted. Fixing then the normalization EM_0 from the requirement to match the observed He-like r flux in oxygen, we can compute the pressure dependent total coronal volume from the formula $V_{\rm tot} = \frac{4k^2 EM_0}{p^2 T_0^2(\alpha+3)}$ and find $V_{\rm tot} = 4^{+7}_{-2} \times 10^{32}$ cm^3; clearly, because of the quadratic dependence of the coronal volume on pressure the errors are still substantial. Nevertheless, the nominal value of $V_{\rm tot} = 4 \times 10^{32}$ cm^3 leads (for an assumed stellar radius of 0.5 $R_\odot$, two identical stars and filling factor of unity) to a height of $\approx 10^{10}$ cm, i.e., about one third of the stellar radius and hence much larger than typical solar coronal loops.

Using the line ratio f/i of the He-like triplets of oxygen and nitrogen one recognizes a trend, indicating lower f/i-ratios and thus lower densities for inactive stars. This conclusion has, however, to be treated with some care. The available data support it only for main sequence stars, i.e., for YY Gem, AD Leo, and ϵ Eri do we measure f/i-ratios significantly below the low-density limit. For Algol the measured low f/i-ratio does not necessarily imply high densities, in principle it can also be attributed to a special geometrical configuration immersing its corona in the radiation field of its B-type companion (cf.

Sect. 5.1). For UX Ari the data are consistent with the low density limit, but because of the large errors significant f/i ratios can also not be ruled out. Only for Capella the measurement errors are small enough that we can state with confidence that the measured f/i-ratio places Capella very close to the low-density limit. For Capella one can definitely exclude densities as high as $10^{13}\,\mathrm{cm}^{-3}$, which were reported by Dupree et al. (1993) from EUVE measurements of Fe XXI lines, which are, however, formed at a much higher temperature than O VII. The analysis of the long wavelength portion of the *Chandra* LETGS spectrum by Mewe et al. (2001) yielded only upper limits of $\approx 2 \times 10^{12}\,\mathrm{cm}^{-3}$ for Fe XXI, and similarly for their He-like line ratios of Mg XI and Si XIII no significant densities could be derived. The densities derived from N VI show the same trend as those derived from oxygen. Again we emphasize that the peak of the emission measure distribution for the most active stars lies above the peak formation temperatures of those specific ions. For the lowest temperature ion, C V, the f/i-ratios for the hotter stars are dominated by radiation effects; also higher order line blending limits the accuracy with which the C V-triplet can be determined. In all cases where the C V-triplet could be detected f/i-ratios of approximately unity were found. The higher Z ions Ne to Si are more difficult to study with the LETGS, since they are not fully resolved and line blending occurs especially for Ne IX. These line blends can still be modelled and thus de-blended, but our results should be confirmed with higher resolution measurements available with, e.g., the MEG. The mean X-ray surface flux appears to be a useful parameter segregating stars into different levels of activity; another useful parameter appears to be the ratio between Ly_α line flux and the He-like triplet resonance line flux, especially for oxygen. A grouping of stars is apparent when mean X-ray surface flux and the ratio between Ly_α and He-like triplet flux are considered. Larger data samples are required to assess any physical significance of such groupings and open the road to an X-ray "HR-diagram".

Acknowledgements. J.-U.N. acknowledges financial support from Deutsches Zentrum für Luft- und Raumfahrt e.V. (DLR) under 50OR98010.
The Space Research Organization Netherlands (SRON) is supported financially by NWO.

References

Antunes, A., Nagase, F., & White, N. E. 1994, ApJ, 436, L83
Audard, M., Güdel, M., & Mewe, R. 2001a, A&A, 365, L318
Audard, M., Behar, E., Güdel, M., et al. 2001b, A&A, 365, L329
Audard, M., Güdel, M., & Sres, A. 2001c, Tysc. Conf, 102
Ayres, T. R., Brown, A., Osten, R. A., et al. 2001, ApJ, 549, 554
Blumenthal, G. R., Drake, G. W., & Tucker, W. H. 1972, ApJ, 172, 205
Brinkman, A. C., Behar, E., Güdel, M., et al. 2001, A&A, 365, L324
Brickhouse, N. S., Dupree, A. K., & Young, P. R. 2001, A&AS, 19911202
Canizares, C. R., Huenemoerder, D. P., Davis, D. S., et al. 2000, ApJ, 539, L41
Doyle, J. G. 1980, A&A, 87, 183
Dupree, A. K., Brickhouse, N. S., Doschek, G. A., et al. 1993, ApJ, 418, L41
Gabriel, A. H., & Jordan, C. 1969, MNRAS, 145, 241
Gabriel, A. H., Bely-Dubau, F., Faucher, P., et al. 1988, J. Phys., 49, 235
Güdel, M., Audard, M., Briggs, K., et al. 2001a, A&A, 365, L336
Güdel, M., Audard, M., Magee, H., et al. 2001b, A&A, 365, L344
Hünsch, M., Schmitt, J. H. M. M., & Voges, W. 1998, A&A, 132, 155
Hünsch, M., Schmitt, J. H. M. M., Sterzik, M. F., & Voges, W. 1999, A&A, 135, 319
Mason, H. E., Bhatia, A. K., Kastner, S. O., et al. 1984, Sol. Phys., 92, 199
McKenzie, D. L., & Landecker, P. B. 1982, ApJ, 259, 372
Mewe, R., & Schrijver, J. 1978, A&A, 65, 99
Mewe, R., Gronenschild, E. H. B. M., & van den Oord, G. H. J. 1985, A&AS, 62, 197
Mewe, R., Kaastra, J. S., & Liedahl, D. A. 1995, Legacy, 6, 16 (MEKAL)
Mewe, R., Raassen, A. J. J., Drake, J. J., et al. 2001, A&A, 368, 888
Ness, J.-U., Mewe, R., Schmitt, J. H. M. M., et al. 2001a, A&A, 367, 282
Ness, J.-U., Mewe, R., Schmitt, J. H. M. M., et al. 2001b, ASP Conf. Ser., in press (poster at Stellar Coronae 2001)
Ness, J.-U., Mewe, R., Schmitt, J. H. M. M., et al. 2001c, PASP, in press (presentation at Cool Stars workshop CS12)
Ness, J.-U., Schmitt, J. H. M. M., Burwitz, V., et al. 2002a, A&A, 387, 1032
Ness, J.-U., Brickhouse, N., Drake, J. J., et al. 2002b, in preparation
Ness, J.-U., & Wichmann, R. 2002, Astron. Nachr. 323, 2, 129 (CORA program)
Pallavicini, R., Golub, L., Rosner, R., et al. 1981, ApJ, 248, 279
Pease, D. O., Drake, J. J., Johnson, C. O., et al. 2000, SPIE, 4012, 700 Effective areas for the LETGS measured Oct. 31, 2000, downloaded from `http://asc.harvard.edu/cal/Links/Letg/User/`
Phillips, K. J. H., Mathioudakis, M., Huenemoerder, D. P., et al. 2001, MNRAS, 325, 1500
Porquet, D., Mewe, R., Dubau, J., et al. 2001, A&A, 376, 1113
Pradhan, A. K., & Shull, J. M. 1981, ApJ, 249, 82
Pradhan, A. K., Norcross, D. W., & Hummer, D. G. 1981, ApJ, 246, 1031
Raassen, A. J. J., Mewe, R., Audard, M., et al. 2002a, A&A, 389, 228
Raassen, A. J. J., Ness, J.-U., Mewe, R., et al. 2002b, in preparation
Schmitt, J. H. M. M., Collura, A., Sciortino, S., et al. 1990, ApJ, 365, 704
Schmitt, J. H. M. M. 1997, A&A, 318, 215
Schmitt, J. H. M. M. 1998, ASP Conf. Ser., 154, 463
Schmitt, J. H. M. M., & Ness, J.-U. 2002, A&A, 388, L13
Schrijver, C. J., Mewe, R., & Walter, F. M. 1984, A&A, 38, 258
Stelzer, B., Burwitz, V., Audard, M., et al. 2002, A&A, accepted
Vaiana, G. S., Cassinelli, J. P., Fabbiano, G., et al. 1981, ApJ, 245, 163